Development of a Simultaneous Continuum and Noncontinuum State Estimator with Application on a Distillation Process

Moshood J. Olanrewaju, Biao Huang, and Artin Afacan
Dept. of Chemical and Materials Engineering, University of Alberta, Edmonton, Alberta, Canada T6G 2G6

DOI 10.1002/aic.12605
Published online April 15, 2011 in Wiley Online Library (wileyonlinelibrary.com).

This study focuses on the development and application of a hybrid moving horizon estimator (HMHE) to achieve simultaneous estimation of both continuum and noncontinuum states in a constrained switching dynamic system. One of the major issues in a moving horizon estimation approach is the development of an arrival cost to summarize the effect of past and a prior *information. In this work, we have developed a generalized arrival cost, which accounts for both continuum and noncontinuum states. A generalized hybrid state estimator, which can be used as a stand-alone continuum state estimator, or as a simultaneous continuum and noncontinuum state estimator, is developed. The effects of constraints, process, and measurement noise levels, as well as a moving horizon length on the simultaneous estimation of both the continuum and noncontinuum states are analyzed. The effectiveness of the HMHE is demonstrated through simulation studies, while its practical reliability is tested by conducting experimental studies on a distillation column.* © 2011 American Institute of Chemical Engineers *AIChE J,* 58: 480–492, 2012
Keywords: process control, distillation

Introduction

State estimation of a hybrid system, which consists of the interacting continuum and noncontinuum states, is a significant and challenging problem for process monitoring,[1,2] feedback control,[3–5] and model-based fault diagnosis and isolation.[6] There has been an increased research interest recently in the development and application of a hybrid state estimation to address various problems of interest in hybrid systems.

Alessandri and Coletta[7,8] considered an estimation approach based on Luenberger-like observers for a class of switched continuous and discrete time linear systems with a known operating mode. Böker and Lunze[9] proposed switching Kalman filters for switched affine systems, where a set of Kalman filters is designed for each local dynamics of the hybrid system. An estimation method of combining local observers with Luengerger observers based on known discrete input and output was studied by Balluchi et al.,[3] while Hofbaur and Williams[10] developed a method based on banks of extended Kalman filters, which only focused on the set of most likely modes. Boers and Driessen[1] numerically solved a hybrid state estimation problem using a particle filter approach.

The design and stability analysis of hybrid nonlinear control systems for a class of switched nonlinear systems have also been extensively studied in the literature.[4,5] El-Farra et al.[5] addressed nonlinear and constrained control system of switched systems. In their work, a deterministic high gain observer was developed for estimation of unconstrained states. A predictive control framework for the constrained stabilization of switched nonlinear systems was proposed by

Correspondence concerning this article should be addressed to B. Huang at biao.huang@ualberta.ca.

Mhaskar et al.[4] The key achievement in this work is the design of a Lyaounov-based model predictive controller (MPC) that guarantees the stability of the switched closed-loop system. The Lyaounov-based MPC developed in the work of Mhaskar et al.[4] can be used in combination with a moving horizon based estimation technique, which is the main focus of this work, to develop a more effective nonlinear multivariable control system for a switched system. In one of the most recent studies in hybrid state estimation application in control system design and implementation, Hu and El-Farra[2] explored a technique for fault detection and monitoring of nonlinear hybrid systems with control actuator faults and uncertain mode transitions. The proposed mode observers, which work sequentially with the Lyapunov-based fault detector schemes, are able to identify the active mode without information from the controllers.

There are basically two approaches (i.e., sequential and simultaneous) to a hybrid state estimation development. Sequential approach is a method in which two separate algorithms are combined interactively to estimate both the continuum and noncontinuum states. One distinct feature of this method is the requirement to involve two filters or two objective functions (in the case of optimization based filters), one to estimate the continuum state, while the other to estimate the noncontinuum state.[3,9,11]

Most of the hybrid state estimation methods that exist in the literature use sequential approach largely because it is intuitively the easier of the two approaches to develop or formulate. Besides, combination of different types of filters can be tried to achieve one form of improvement or the other. However, the major setback of this method is the interaction effects of two filters, especially if there are other external constraints desired to be satisfied by the system.[12] Besides, a hybrid state estimation that uses such an approach often poses different implementation challenges. Another approach to a hybrid state estimation development is called a simultaneous approach, in which a single filter with a single objective function is formulated to simultaneously estimate both the continuum and noncontinuum states. The development of such a filter is nontrivial, but it has the advantage of addressing a hybrid state estimation problem in a unified and systematic way. The work presented in this article belongs to the simultaneous approach.

A moving horizon estimation (MHE) is one of the few methods, which provides a platform to develop a simultaneous continuum and noncontinuum states estimation largely because a state estimation problem can be casted as a single optimization function and be readily solved.[12] Bemporad et al.[6] explored the ideas of receding horizon control to the state estimation and fault detection problems of hybrid systems. Ferrari-Trecate et al.[13,14] investigated state estimation for hybrid systems in the mixed logical dynamical form and proposed a state-smoothing algorithm for hybrid systems based on MHE. Sufficient conditions to guarantee asymptotic convergence of the MHE were given. Pina and Botto[15] extended MHE method to simultaneous estimation of state and unknown input for hybrid linear systems.

Rowe and Maciejowski[16] developed a strategy for a min-max MHE of a class of uncertain Piecewise Affine systems (PWA) with both continuous valued and logic components. Their work is an extension of the MHE scheme for PWA systems but without plant uncertainties, as presented in the work of Ferrari-Trecate et al.[13,14] Sufficient conditions that guarantee convergence of the MHE scheme on hybrid systems were also analyzed. In a more recent study, Alessandri et al.[17] used a receding-horizon approach for the estimation of the system mode according to a minimum-distance. In this case, the system and measurement equations of each mode are assumed to be linear and perfectly known, but the current mode of the system is unknown and is regarded as a discrete state to be estimated at each time instant together with the continuous state vector.

The MHE method can simultaneously estimate the state and the mode of the system, and it is based on a moving fixed-size estimation window, which bounds the size of the optimization problem. A state estimation method based on a MHE is able to overcome most of the existing challenges on state estimation problems because it estimates the desired variables over a horizon. Besides, this formulation can take constraints into account explicitly and shape the estimates to form different distributions.[12]

Although, a MHE reduces the computational burden of solving a full information estimation problem by considering a finite horizon of the measurement data, however, the process of summarizing and updating the prior information from the past data (i.e., arrival cost) is nontrivial.[12,18,19] The problem of the arrival cost development will surely be further complicated by the presence of noncontinuum states. This is because the arrival cost for a hybrid moving horizon estimator (HMHE) must not only summarize the past data based on the continuum state evolution but also must be able to account for the past history of the system mode transition trajectory. In one of our recent studies Olanrewaju and Huang, submitted a MHE method was used to develop noncontinuum state estimator. A detailed derivation of an arrival cost for noncontinuum state MHE was provided. When applying the noncontinuum state estimator to the switching dynamic system, a Kalman filter is recommended to approximately reproduce the continuum state to sequentially estimate the noncontinuum state (i.e., switching sequence).

In this study, a generalized hybrid state estimation technique, which is based on a moving horizon approach to achieve a simultaneous estimation of both the continuum and noncontinuum states from a single hybrid objective function, is developed. Arrival cost for a HMHE will be derived. The effects of constraints, process and measurement noise levels, and a moving horizon length on the simultaneous estimation of both the continuum and noncontinuum states will be studied. To test the practical reliability of the proposed estimation method, a detailed experimental work will be carried out on a distillation process to estimate the top product composition as well as the operating mode change due to the switching dynamics in the vapor boilup using the available noisy temperature measurements.

A Hybrid Process Model

Consider the following switching discrete process model:

$$m_k = \eta(m_{k-1};\lambda), x_k = f_{m_k}\{x_{k-1}, u_{k-1};\theta\} + w_{k-1},$$
$$y_k = g_{m_k}(x_k;\beta) + v_k, m_k \in \mathbb{M}: \quad \mathbb{M} = \{1,\ldots,M\}, \quad (1)$$

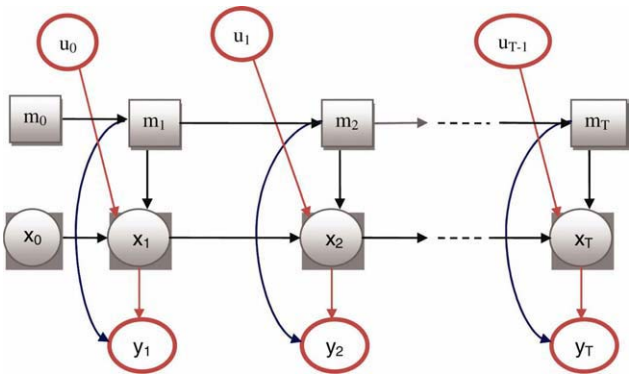

Figure 1. A switched dynamic system with continuum and noncontinuum states.

[Color figure can be viewed in the online issue, which is available at wileyonlinelibrary.com].

where $x_k \in \mathbb{R}^n$ denotes the continuum state, $u_k \in \mathbb{R}^p$ is the input and $y_k \in \mathbb{R}^q$ denotes the observed output from the system. m_k is the noncontinuum state, which denotes the system operating mode. f_{m_k} is a transition function determining the mean of x_k given x_{k-1} and m_k, while g_{m_k} is an output function determining the mean of the y_k given x_k and m_k. $w_k \in N(0, Q_k)$ and $v_k \in N(0, R_k)$ are assumed to be the additive process noise and measurement noise, respectively, while the initial condition is also assumed to be Gaussian, i.e., $x_0 \in N(\overline{x}_0, P_0)$. θ and β denote the system parameters. Change in the system operating mode can be due to either a change in the system internal states, a case that is common in chemical systems with steady state multiplicities,[21] or an unknown external disturbance input.[15,22]

This article focuses only on state estimation of a switched system given that both the output y and input u are known. In this study, we have not considered the control system design for a switched system. We have considered an open loop switched system in most of our simulation and experimental studies. This is evident from the data reported in Table 3. However, in the last section of this work, we considered a situation where information were to be available from a change in the manipulated variable (i.e., input u) and showed how such information can be incorporated in the design of a HMHE in the form of a constraint. The unknown switching transition function (η) for this process, as shown in Figure 1, is assumed to follow a hidden Markov model (HMM) λ, and it is defined as

$$\lambda = \mathrm{HMM}(\mathbb{P}, d_{m_k}(y_k), p_0), \tag{2}$$

where $\mathbb{P}$ is the state transition probability, $d_{m_k}(y_k)$ is the observation probability of y_k given m_k and p_0 is the initial probability of the mode. This article focuses only on state estimation of an open-loop switched system given that both the output measurement and manipulated input are known. In this study, we have not considered the control system design for a switched system. However, in the last section of this work, we considered a situation where available information from a change in the manipulated variable can be incorporated in the design of a HMHE in the form of a constraint to improve both the estimation accuracy.

Hybrid Moving Horizon Estimator (HMHE)

If we define $x_{0:T} = \{x_0,\ldots,x_T\}$ and $m_{0:T} = \{m_0,\ldots,m_T\}$, then, a hybrid batch state estimation can be formulated as the optimum sequences of the continuum and noncontinuum states for which the conditional joint probability density function (*jpdf*) $P(m_{0:T},x_{0:T}|y_{0:T})$ is maximized or equivalently, for which the negative logarithm of the *jpdf* $P(m_{0:T},x_{0:T},y_{0:T})$ is minimized:

$$\min_{\hat{m}_{0:T},\ \hat{x}_{0:T}} J_T: \quad J_T := -\ln P(m_{0:T}, x_{0:T}, y_{0:T}). \tag{3}$$

However, instead of using all of the available measurements $y_{0:T}$ to solve for the optimum state sequence $\hat{m}_{0:T}$ and $\hat{x}_{0:T}$ through a batch optimization, we propose a rigorous formulation of a HMHE objective function, which seeks to optimize the negative logarithm of the joint distribution of the states $x_{T-N:T}$ and $m_{T-N:T}$ given all of the measurement data up to time T as

$$\min_{\hat{m}_{T-N:T},\ \hat{x}_{T-N:T}} \{J_T\}: \quad J_T = -\ln P(x_{T-N:T}, m_{T-N:T}, y_{0:T}). \tag{4}$$

J_T can also be expressed as

$$J_T = -\ln P(x_{T-N}, m_{T-N}, y_{0:T-N}) - \ln P(x_{T-N+1:T}, m_{T-N+1:T}, y_{T-N+1:T}|x_{T-N}, m_{T-N}, y_{0:T-N}). \tag{5}$$

However, given the fact that $x_{T-N+1:T}$,$m_{T-N+1:T}$ and $y_{T-N+1:T}$ are conditionally independent on $y_{0:T-N}$, given x_{T-N} and m_{T-N} (see Figure 1, and using the Markov property), 5 can be reduced to

$$J_T = -\ln P(x_{T-N}, m_{T-N}, y_{0:T-N}) - \ln P(x_{T-N+1:T}, m_{T-N+1:T}, y_{T-N+1:T}|x_{T-N}, m_{T-N}). \tag{6}$$

If we define each term of 6 as follows:

$$\phi_{T-N} = -\ln P(x_{T-N}, m_{T-N}, y_{0:T-N}), \tag{7}$$

and

$$J_{T-N+1:T} = -\ln P(x_{T-N+1:T}, m_{T-N+1:T}, y_{T-N+1:T}|x_{T-N}, m_{T-N}), \tag{8}$$

then, 4 can be simplified as

$$\min_{\hat{m}_{T-N:T},\ \hat{x}_{T-N:T}} \{J_T\}: \quad J_T = \phi_{T-N} + J_{T-N+1:T}, \tag{9}$$

Using a Markov property,[23] the HMHE objective function can be derived from 9 as shown in Appendix A to give

$$\min_{\{\hat{m}_{T-N:T},\ \hat{w}_{T-N:T}\}} J_T : J_T = \phi_{T-N} - \sum_{k=T-N+1}^{T}\sum_{i=1}^{M}\sum_{j=1}^{M}\gamma_{k-1}^{(i)}\alpha_k^{(j)} \ln \mathbb{P}_{k-1,k}^{(i,j)} + \sum_{k=T-N}^{T-1}\sum_{j=1}^{M}\alpha_k^{(j)}\hat{w}_k^T Q_k^{-1}\hat{w}_k + \sum_{k=T-N+1}^{T}\sum_{j=1}^{M}\alpha^{(j)}\hat{v}_k^T R_k^{-1}\hat{v}_k, \tag{10}$$

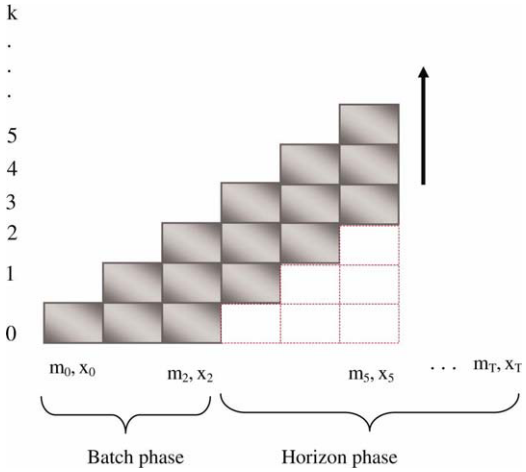

Figure 2. Batch and horizon phases.

[Color figure can be viewed in the online issue, which is available at wileyonlinelibrary.com].

subject to:

$$\hat{x}_k = f_{\hat{m}_k}(\hat{x}_{k-1}, u_{k-1}; \theta) + \hat{w}_{k-1}, \qquad k = T-N : T-1,$$
$$\hat{v}_k = y_k - g_{\hat{m}_k}(\hat{x}_k; \beta), \qquad k = T-N : T,$$
$$\gamma_{k-1}^{(i)} = \begin{cases} 1 & \text{if } i = \hat{m}_{k-1} \\ 0 & \text{if } i \neq \hat{m}_{k-1}, \end{cases} \qquad \alpha_k^{(j)} = \begin{cases} 1 & \text{if } j = \hat{m}_k \\ 0 & \text{if } j \neq \hat{m}_k, \end{cases}$$
$$\hat{m}_k \in \mathbb{M}: \qquad \mathbb{M} = \{1, \ldots, M\}. \quad (11)$$

ϕ_{T-N} in 10 is the cost at time $T-N$, given all of the observations up to time $T-N$. The term ϕ_{T-N} will be referred to as the arrival cost, which means the cost associated with the uncertainty of continuum and noncontinuum states at time $T-N$, given all the observed outputs up to time $T-N$, the beginning of the horizon phase. By examining 10 and 11, one can interpret a MHE as an approach that tries to preserve the old information through the description of the uncertainty in the first term of 10 while using the most recent N + 1 measurements over a sliding horizon window as shown in Figure 2 to achieve the desired optimum estimation of all the states within the window.

Arrival cost

Arrival cost is important to a MHE approach because it summarizes the effect of the past processed data on the estimation of the current states.[12] Intuitively, the arrival cost as defined in 7 accounts for two things: (1) the cost associated in part with the uncertainty in the estimated noncontinuum state $\hat{m}_{T-N}$ being in mode $l \in \{1,\ldots,M\}$ and (2) the cost associated in part with the uncertainties in the estimated continuum state $\hat{x}_{T-N}$.

The arrival cost in 7 can be expanded as follows:

$$\phi_{T-N} = -\ln[P(x_{T-N}|m_{T-N}, y_{0:T-N})P(m_{T-N}, y_{0:T-N})] = \phi_{T-N}^{x} + \phi_{T-N}^{m}, \quad (12)$$

where $\phi_{T-N}^{x} = -\ln P(x_{T-N}|m_{T-N}, y_{0:T-N})$, is the arrival cost in part, due to the uncertainty in the continuum state and $\phi_{T-N}^{m} = -\ln(P(m_{T-N}, y_{0:T-N})$, is the arrival cost in part, due to the uncertainty in the the noncontinuum state at time $T-N$.

Arrival Cost: ϕ_{T-N}^{m}. While various forms of arrival cost of a MHE for a continuous-valued system have been well explored in the literature,[12,18,19] little attention has been given to arrival cost development of a moving horizon based approach to noncontinuum state estimation. In this section, we will present the arrival cost due to the noncontinuum state transition by considering the second term of 12 as follows:

$$\phi_{T-N}^{m}(j) = -\ln P(m_{T-N}, y_{0:T-N}), \quad (13)$$

where $\phi_{T-N}^{m}(j)$ is the cost of arriving at state $m_{T-N} = j$ at time $T-N$ given all of the measurements up to time $T-N$. A recursive solution of 13 can be derived using a forward procedure technique Olanrewaju and Huang, submitted to obtain

$$\phi_{T-N}^{m}(j) = \sum_{i=1}^{M} [\phi_{T-N-1}(i) - \ln \mathbb{P}_{T-N-1,T-N}^{(i,j)}] - \ln P(y_{T-N}|m_{T-N} = j). \quad (14)$$

Under the assumption of a Gaussian distribution, the conditional distribution density function $P(y_{T-N}|m_{T-N} = j)$ from the 14 can be expressed as

$$P(y_{T-N}|m_{T-N}) = (2\pi)^{-\frac{q}{2}} R_{T-N}^{-\frac{1}{2}} \exp\left[-\frac{1}{2}\{y_{T-N} - g_{m_{T-N}}(x_{T-N}; \beta)\}^T R_{T-N}^{-1}\{y_{T-N} - g_{m_{T-N}}(x_{T-N}; \beta)\}\right]. \quad (15)$$

Therefore, the last term in 14 will become

$$-\ln P(y_{T-N}|m_{T-N} = j) = \mathbf{C}_{T-N} + \frac{1}{2} v_{T-N}^T R_{T-N}^{-1} v_{T-N}, \quad (16)$$

where $\mathbf{C}_{T-N} = -\ln(2\pi)^{-\frac{q}{2}} R_{T-N}^{-\frac{1}{2}}$ and $v_{T-N} = y_{T-N} - g_{m_k}(x_{T-N}; \beta)$. By substituting 16 into 14, we have the following cost function:

$$\phi_{T-N}^{m}(j) = \underbrace{\sum_{i=1}^{M} [\phi_{T-N-1}(i) - \ln \mathbb{P}_{T-N-1,T-N}^{(i,j)}]}_{\text{Arrival cost based on past data}} + \underbrace{\frac{1}{2} v_{T-N}^T R_{T-N}^{-1} v_{T-N} + \mathbf{C}_{T-N}}_{\text{Cost based on current data at } T-N}. \quad (17)$$

Arrival Cost: ϕ_{T-N}^{x}. In this section, we shall derive the first term of 12, which is given as follows

$$\phi_{T-N}^{x} = -\ln P(x_{T-N}|m_{T-N}, y_{0:T-N}). \quad (18)$$

The derivation of an equivalent but recursive optimum solution of 18 for a constrained dynamic system is difficult to achieve analytically. However, for an unconstrained hybrid linear system, the recursive form of 18 is a well-known switching Kalman filter.[9,12] Let us first consider an unconstrained switching linear system of the form

$$x_k = F_{(m_k)}x_{k-1} + w_k \quad w_k \in N(0, Q_k),$$
$$y_k = H_{(m_k)}x_k + v_k \quad v_k \in N(0, R_k). \tag{19}$$

At any given time k and the noncontinuum state m_k, 18 reduces to

$$\phi_k^x = -\ln P(x_k|m_k, y_{0:k}). \tag{20}$$

where ϕ_k^x is the cost due to the uncertainties in the continuum state given the observation sequence up to time k. Following the work of Rao and Rawlings,[12] we can derive the cost function of 20 at any given time k as

$$\phi_k^x = \underbrace{\frac{1}{2}\hat{w}_{k-1}^T P_k^{-1}\hat{w}_{k-1}}_{\text{Arrival cost based on past data}} + \underbrace{\frac{1}{2}\hat{v}_k^T R_k^{-1}\hat{v}_k}_{\text{Observation cost at time } k} + \mathbf{E}_k. \tag{21}$$

The derivation of 21 from 20 as well as the definition of the parameter $\mathbf{E}_k$ are detailed in Appendix B. For a nonlinear hybrid system, an approximate extended switching Kalman filter has to be employed and the P_k will be evaluated[12] as

$$P_k = F_k P_{k-1} F_k^T + Q_{k-1} - F_k P_{k-1} H_k (H_k P_{k-1} H_k^T + R_k)^{-1} H_k P_{k-1} F_k^T, \tag{22}$$

where F_k and H_k are evaluated along the estimated trajectories according to the following equations:

$$F_k = \frac{\partial f_{\hat{m}_k}(\hat{x}_{k-1}, u_{k-1}; \theta)}{\partial x_k}, \tag{23}$$

$$H_k = \frac{\partial g_{\hat{m}_k}(\hat{x}_k; \beta)}{\partial x_k}. \tag{24}$$

In a similar way, the cost function at the time $T - N$, which is a recursive form of 21 can be written as

$$\phi_{T-N}^x = \underbrace{\frac{1}{2}\hat{w}_{T-N-1}^T P_{T-N}^{-1}\hat{w}_{T-N-1}}_{\text{Arrival cost based on past data}} + \underbrace{\frac{1}{2}\hat{v}_{T-N}^T R_{T-N}^{-1}\hat{v}_{T-N}}_{\text{Observation cost at } k=T-N} + \mathbf{E}_{T-N}, \tag{25}$$

A generalized HMHE

By substituting 17 and 25 into the 10, a generalized HMHE can be formulated as

$$\min_{\{\hat{m}_{T-N:T},\ \hat{w}_{T-N-1:T-1}\}} J_T : J_T = \sum_{j=1}^{M}\sum_{i=1}^{M} \alpha_{T-N}^{(j)} \gamma_{T-N-1}^{(i)} [\phi_{T-N-1}(i) - \log \mathbb{P}_{T-N-1,T-N}^{(i,j)}] + \hat{w}_{k-N-1}^T \bar{P}_{k-N}^{-1} \hat{w}_{k-N-1} - \sum_{k=T-N+1}^{T}\sum_{i=1}^{M}\sum_{j=1}^{M} \gamma_{k-1}^{(i)} \alpha_k^{(j)} \ln \mathbb{P}_{k-1,k}^{(i,j)} \sum_{k=T-N}^{T-1}\sum_{j=1}^{M} \alpha_k^{(j)} \hat{w}_k^T \bar{Q}_k^{-1} \hat{w}_k + \sum_{k=T-N}^{T}\sum_{j=1}^{M} \alpha^{(j)} \hat{v}_k^T \bar{R}_k^{-1} \hat{v}_k, \tag{26}$$

subject to:

$$\hat{x}_k = f_{\hat{m}_k}(\hat{x}_{k-1}, u_{k-1}; \theta) + \hat{w}_{k-1}, \qquad k = T-N : T-1,$$
$$\hat{v}_k = y_k - g_{\hat{m}_k}(\hat{x}_k; \beta), \qquad k = T-N : T,$$
$$\gamma_{k-1}^{(i)} = \begin{cases} 1 & \text{if } i = \hat{m}_{k-1} \\ 0 & \text{if } i \neq \hat{m}_{k-1}, \end{cases} \quad \alpha_k^{(j)} = \begin{cases} 1 & \text{if } j = \hat{m}_k \\ 0 & \text{if } j \neq \hat{m}_k, \end{cases}$$
$$\hat{m}_k \in \mathbb{M}: \quad \mathbb{M} = \{1, \ldots, M\}. \tag{27}$$

where $\overline{P}_{k-N}^{-1} = \frac{1}{2}P_{K-N}^{-1}, \bar{Q}_k^{-1} = \frac{1}{2}Q_k^{-1}$, and $\bar{R}_k^{-1} = \frac{1}{2}R_k^{-1}$. Note that the parameters $\mathbf{C}_{T-N}$ and $\mathbf{E}_{T-N}$ have been neglected in the final form of HMHE in 26 because they are independent of the decision variables in the optimization function. The objective function of 26 and 27 constitutes a mixed integer nonlinear programming (MINLP) problem.

For simplicity, the general form of the MINLP problem can be posed as

$$\min_{x,m} J_T = f(x, m), \tag{28}$$

subject to:

$$g(x, m) \leq 0,$$
$$x \in \mathbb{X}, \tag{29}$$
$$m \in \mathbb{M}, \qquad \text{(Integer)}.$$

The function $f(x, m)$ is a nonlinear objective function and $g(x, m)$ is a nonlinear constraint function. The variables, x and m, are the decision variables, where m is required to be integer taking discrete values in the space $\mathbb{M} = \{1,\ldots,M\}$. Any decision variables $\{x, m\}$ satisfying the constraints of 29 is called a feasible point of 28.[23] Any feasible point, whose objective function value is less than or equal to that of all other feasible points, is called optimal solution. The continuous variables in 28 could, for instance, describe the states (i.e., concentration, temperature, and pressure), flow rates or design parameters of a chemical process. The discrete variables, may be used to describe a change in system operating modes, the existence or nonexistence of process faults, and stiction or nonstiction of control valves.

There are different methods that have been developed in the literature to solve MINLP problems. Some of the solution methods include branch-and-bound (B&B),[24] combinatorial mixed-integer optimization,[23,25] outer approximation (OA),[26,27] extended cutting plane,[23] and a generalized benders decomposition (GBD).[28] Most of these approaches generally rely on the successive solutions of closely related nonlinear problems (NLP).[23] In this work, we have employed a combinatorial mixed-integer optimization approach[23,25] to provide the solution for MINLP problem of 28 and 29.

State constraints

One of the major advantages of a moving horizon state estimation formulation is the ability to handle system constraints. Constraints are typically used to model bounded variables (i.e., states, input, or disturbance). Besides, other additional information about a system can be easily casted in the form of constraints to improve state estimation performance. Constraint handling on a continuum state estimation

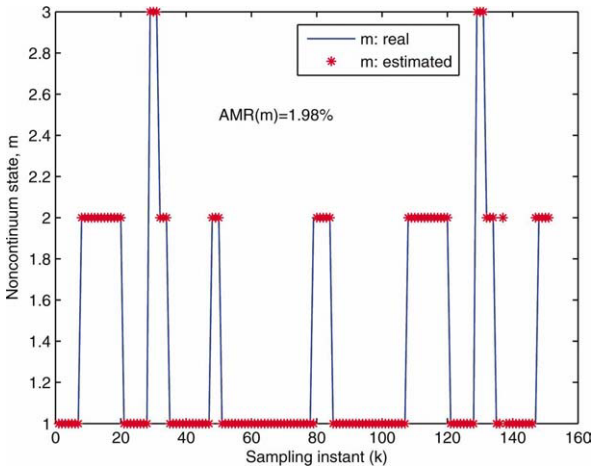

Figure 3. Noncontinuum state estimation: m; δ_w = [03.0;3.0]; δ_v = [3.0;3.0], N = 2.

[Color figure can be viewed in the online issue, which is available at wileyonlinelibrary.com].

through a moving horizon optimization has been well studied. In this work, we demonstrate that additional information about a system can be used to constrain the system operating modes space. For illustration purposes, we consider the following additional constraints as

$$u_k \in \mathbb{U},\ M_i = f(u_k),\ m_k \in \{1, \ldots, M_i\}, \tag{30}$$

$$x_k \in \mathbb{X}, \tag{31}$$

$$w_k \in \mathbb{W}. \tag{32}$$

In this case, the system operating modes space M_i is time varying as its value at any given time k depends on the control input sequences.

Hybrid state estimator performance index

To quantify the performance and accuracy of the developed HMHE, two different types of error criteria are used, which are:

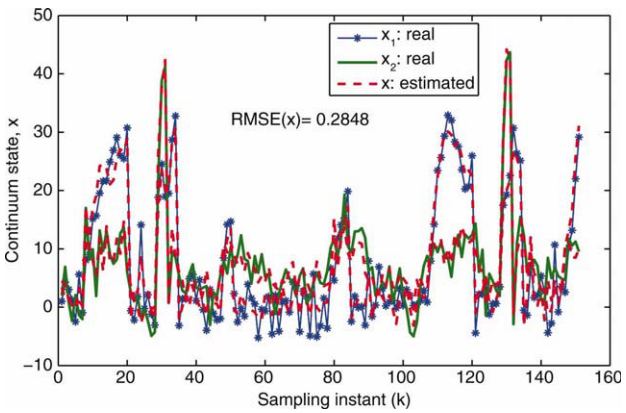

Figure 4. Continuum state estimation: x; δ_w = [3.0;3.0]; δ_v = [3.0;3.0], N = 2.

[Color figure can be viewed in the online issue, which is available at wileyonlinelibrary.com].

Figure 5. Noncontinuum state estimation: m; δ_w = [10.0;10.0]; δ_v = [3.0;3.0], N = 2.

[Color figure can be viewed in the online issue, which is available at wileyonlinelibrary.com].

- Average Missing Rate (AMR): This factor quantifies the performance of the HMHE with respect to noncontinuum state estimation. It expresses, in term of percentage, how well the state estimation is able to capture the change in system modes. The AMR is defined as

$$\text{Missing Rate (AMR)} = \frac{\text{Total number of false estimations}}{\text{Total number of sampling instants}}\%. \tag{33}$$

For instance, an AMR of 0% means we have a perfect estimation with no misclassified points, while 100% implies all of the state operating modes at all sampling instances are identified incorrectly.

- Root Mean Square Error (RMSE): This factor quantifies the differences between estimated and the true values of continuum states. The RMSE is defined as

$$\text{RMSE} = \sqrt{\frac{\sum_{k=1}^{i=T}(x_k - \hat{x}_k)^2}{T}}. \tag{34}$$

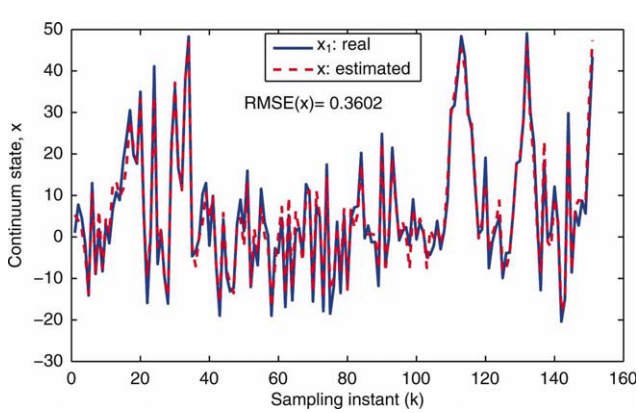

Figure 6. Continuum state estimation: x; δ_w = [10.0;10.0]; δ_v = [3.0;3.0], N = 2.

[Color figure can be viewed in the online issue, which is available at wileyonlinelibrary.com].

Table 1. Effects of the Noise Level, Horizon Length, and Constraint Handling on the HMHE Performance

	Noise Parameters δ_w, δ_v	$N = 1$ AMR, RMSE, Time (%), (x), (min)	$N = 2$ AMR, RMSE, Time (%), (x), (min)
Constraint. $\{M_i\}$ is varying	3, 3	1.987, 0.2848, 0.90	1.987, 0.2848, 3.41
	3, 10	16.55, 0.7407, 0.76	13.24, 0.6814, 2.76
	10, 3	19.86, 0.3604, 1.09	18.54, 0.3602, 4.54
Unconstraint. $\{M_i\}$ is fixed	3, 3	1.987, 0.2848, 1.08	1.987, 0.2848, 4.32
	3, 10	18.54, 0.7964, 0.91	14.56, 0.7273, 3.48
	10, 3	20.53, 0.3566, 1.31	18.55, 0.3562, 5.88

Simulation Studies

A hybrid linear system

In this section, the performance of the developed HMHE will be assessed through a simulation example on a simple linear system switching between two modes as

$$\begin{aligned} m_k &= \eta(m_{k-1};\lambda),\\ x_k &= F^{(m_k)}x_{k-1} + B^{(m_k)}u_{k-1} + w_k, \quad w_k \in N(0,Q_k),\\ y_k &= H^{(m_k)}x_k + v_k, \quad v_k \in N(0,R_k). \end{aligned} \tag{35}$$

The system parameters as well as the hidden Markov parameters are given in the Appendix C. To assess the performance of the HMHE in presence of constraints, the following constraints are incorporated:

$$\begin{aligned} &u_k < 0, && m_k \in M_i: \quad M_i = \{1,2\},\\ &u_k \geq 0, && m_k \in M_i: \quad M_i = \{1,2,3\},\\ &-L\delta_w \leq w_k \leq L\delta_w. \end{aligned} \tag{36}$$

where $L \geq 1$ is a tuning parameter for the continuum state constraint and the last inequality specifies constraint on continuum disturbances.

In this example, the objective is to simultaneously estimate the continuum state $\hat{x}_k$ as well as the noncontinuum state $\hat{m}_k$ given noisy measurements. The measurement noise covariance matrix R_k and state noise covariance matrix Q_k are given as

$$Q_k = \begin{pmatrix} \delta_{w,1}^2 & 0 \\ 0 & \delta_{w,2}^2 \end{pmatrix}, \quad R_k = \begin{pmatrix} \delta_{v,1}^2 & 0 \\ 0 & \delta_{v,2}^2 \end{pmatrix}, \tag{37}$$

where $\delta_{w,i}$ and $\delta_{v,i}$ are the standard deviation of the process and measurement noise, respectively.

The simulated results in Figures 3–6 show the performance of the developed HMHE. Figures 3 and 4 show the estimation performance with both process and measurement noise being the standard deviation of 3, while Figures 5 and 6 show that the hybrid state estimation performance when the standard deviation of the process is increased from 3 to

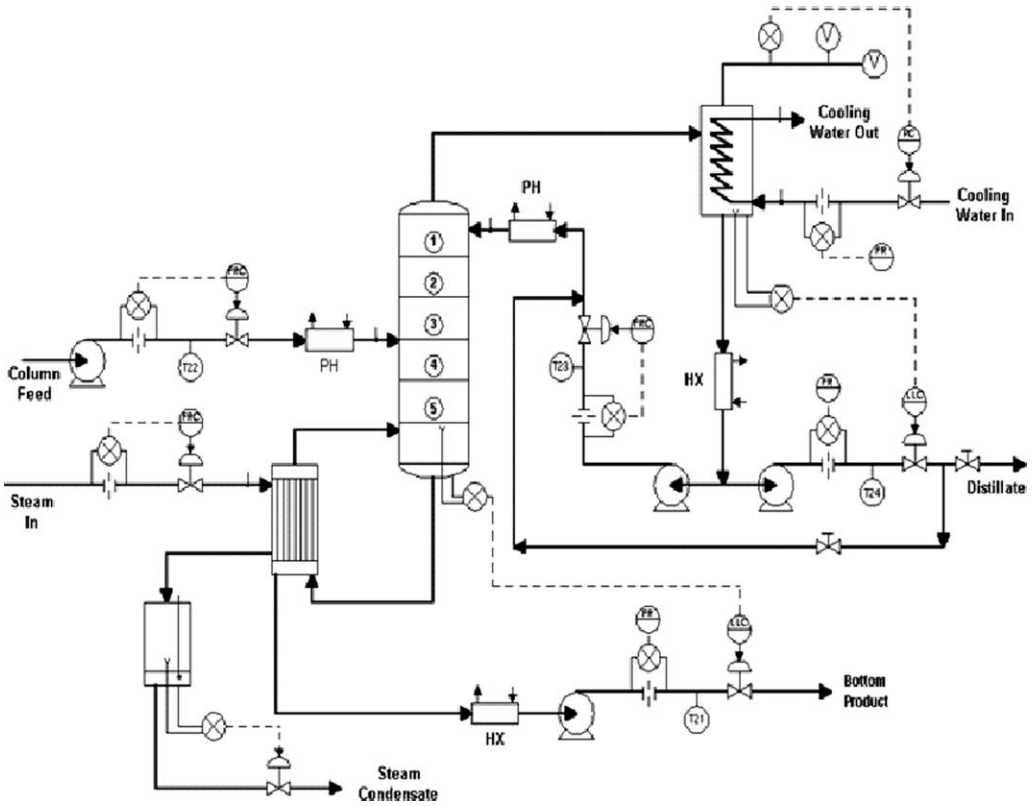

Figure 7. A continuous distillation column setup.

Table 2. Detailed Dimensions of the Column and Trays

Column diameter	0.3 m
Tray active area	0.0537 m^2
Hole diameter	4.76×10^{-3} m
Open hole area	0.00537 m^2
Tray thickness	3.0×10^{-3} m
Outlet weir height	0.063 m
Inlet weir height	0.051 m
Weir length	0.213 m
Liquid path length	0.202 m
Tray spacing	0.457 m

10. It can be seen that the state estimator tracks well the continuum state dynamics, while correctly estimating the change in the system operating modes. However, to quantitatively assess the performance of a simultaneous continuum and noncontinuum state estimation developed, the effect of the noise level (in both the process and measurements), the horizon length N and the constraints on the noncontinuum state space M_i are further examined.

Using the performance index defined in the 33 and 34, the HMHE performances are analyzed and summarized in Table 1. The results indicate that using the additional known information of the system to bound the noncontinuum state space will improve both the accuracy of continuum and noncontinuum states estimation. Besides, we can also see from the results of Table 1 that constraining the noncontinuum state space leads to a reduction in the computational time.

Using a MHE naturally offers us one more degree of freedom, which is the availability of the horizon length N as a tuning parameter. From the results in Table 1, it is clear that increasing the horizon length will increase the state estimation performance, though it comes at the expense of the computational time. Therefore, a trade-off has to be reached in selecting the horizon length N to give the desired level of state estimation accuracy for which an acceptable computational time is feasible.

Experimental Study

Online state estimation to a distillation column

State estimation problems can be verified from pilot-scale experiments owing to relatively easy measurement of state variables in pilot scale processes. In this work, we study the performance of a simultaneous continuum and noncontinuum state estimator on a distillation process. There have been a lot of research interests on the application of state estimation to composition monitoring in a distillation process. But only few papers have verified their developed state estimators on the actual experimental data.[11,29–31] Besides, the demand in achieving simultaneous estimation of column composition profiles, operating mode change detection, and fault detection and isolation, are among several factors that necessitate the application of advanced hybrid filters to a distillation process monitoring and control. A hybrid state estimator will also provide a better estimates of the key process variables in an industrially operated distillation column with steady state multiplicities[20,32] and unmeasured disturbance inputs.[33]

Table 3. Operating Modes based on Different Vapor Boil up Rates

Variables	Mode 1	Mode 2	Mode 3
Vapor boilup, V_m (kmol/h)	5.33	6.20	6.91
Reflux flow rate, R_m (kmol/h)	3.51	3.51	3.51
Distillate flow rate, D_m (kmol/h)	1.44	2.80	4.02
Feed flow rate, F_m (kmol/h)	5.89	5.89	5.89
Distillate composition of MeOH, x_D	0.8877	0.8577	0.8217
Feed composition of MeOH, z_m	0.6269	0.6269	0.6269

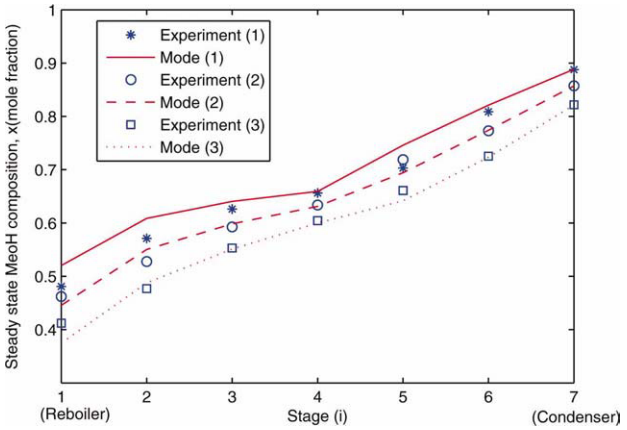

Figure 8. Steady state MeOH composition profiles for different operating modes.

[Color figure can be viewed in the online issue, which is available at wileyonlinelibrary.com].

Distillation process

A distillation column with 0.3 m diameter was used to separate a methanol and isopropanol mixture. A schematic diagram of the experimental setup is shown in Figure 7. The column contains five identical sieve trays and spaced 0.457 m apart. Each tray is made of stainless steel and equipped with thermocouple and liquid sampling point at the outlet of the tray. The top two sections of the column are made of Pyrex

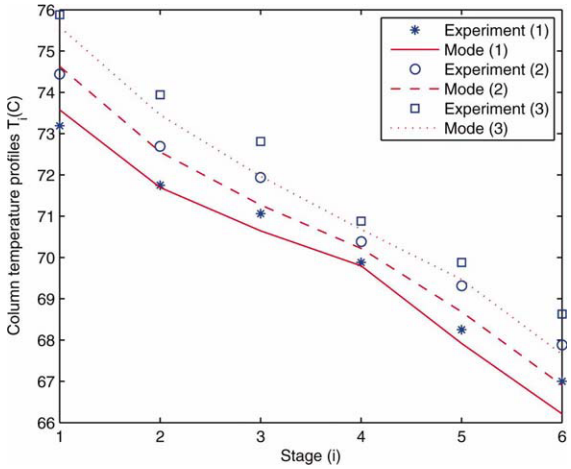

Figure 9. Steady state MeOH temperature profiles for different operating modes.

[Color figure can be viewed in the online issue, which is available at wileyonlinelibrary.com].

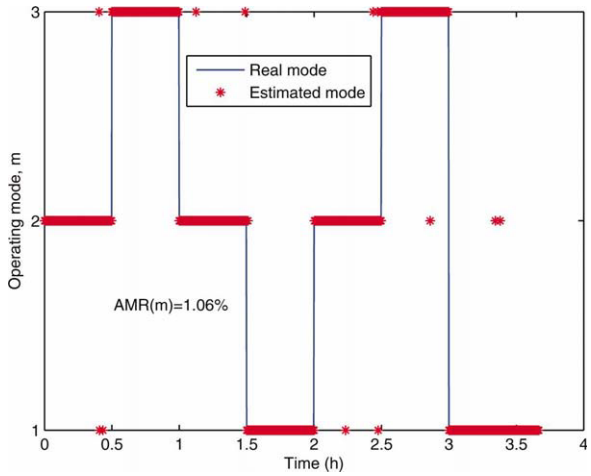

Figure 10. Noncontinuum state estimation: operating mode (m).

[Color figure can be viewed in the online issue, which is available at wileyonlinelibrary.com].

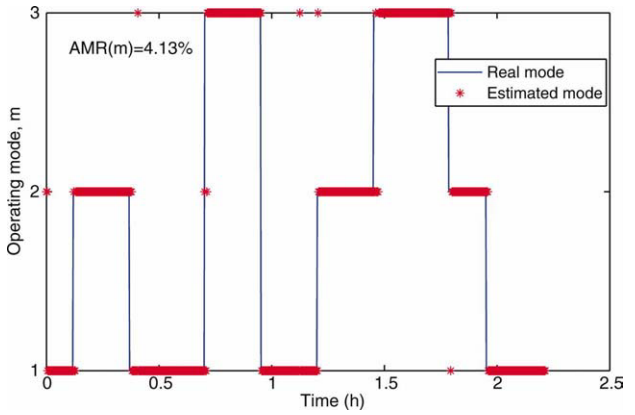

Figure 12. Noncontinuum state estimation: operating mode (m).

[Color figure can be viewed in the online issue, which is available at wileyonlinelibrary.com].

glass to enable observation of the vapor/liquid phenomena; the rest are made of stainless steel. Detailed dimensions of the column and tray are shown in Table 2. The total pressure drop for two trays is measured using a Rosemount differential pressure cell. A total condenser and a thermosiphon partial reboiler complete the distillation system. The column is instrumented for continuous unattended operation. An Opto-22 process I/O subsystem interface with a personal computer running LabView (Version 7.1) software was used for process control and data acquisition. The liquid samples were analyzed using a Hewlett Packard 5790A series II gas chromatograph with a thermal conductivity detector having a column (3.17×10^{-3} m-i.d.) packed with Carbopack.

The column was started with total reflux operation and was then switched to continuous mode by introducing feed to the column and withdrawal of two products from the top and bottom of the column. In this study, a total of three different steady state operating modes were carried out under ambient pressure using methanol-isopropanol mixture. For each operating mode, the reflux flow rate, R_m, feed flow rate, F_m, and methanol composition in the feed, z_m, were kept constant while the only vapor boilup rate was varied. Table 3 shows the operating variables for three steady state operating modes. When the flow rate and temperature profiles shown by the software (LabView) remained constant for a period of 60 min, steady state condition was assumed for that particular mode. Triplicate liquid samples from each tray outlet and condenser bottom as well as one from the reboiler were taken and analyzed to minimize the measurement error. The liquid samples were also taken at 3 min time intervals only from the bottom of the condenser during the transition period between operating modes. For the steady state and transition period between two mode runs, the sampling time was set to 10 s.

Process Model. The development of a state estimation requires a process model. For the distillation process under

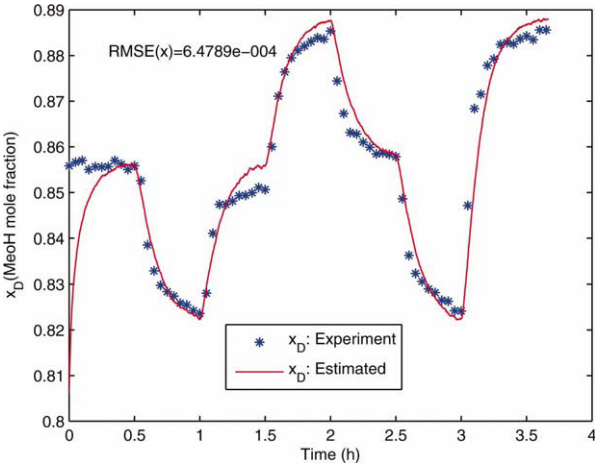

Figure 11. Continuum state estimation: Composition of MeOH in the distillate product.

[Color figure can be viewed in the online issue, which is available at wileyonlinelibrary.com].

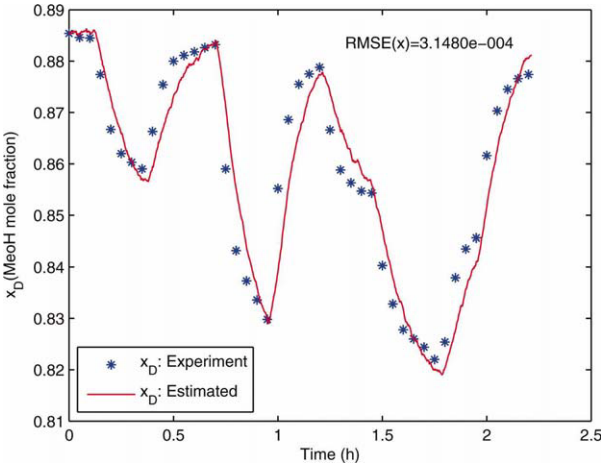

Figure 13. Continuum state estimation: Composition of MeOH in the distillate product.

[Color figure can be viewed in the online issue, which is available at wileyonlinelibrary.com].

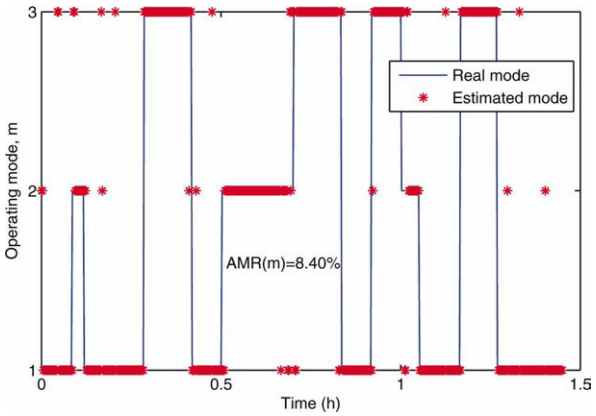

Figure 14. Noncontinuum state estimation: operating mode (m).

[Color figure can be viewed in the online issue, which is available at wileyonlinelibrary.com].

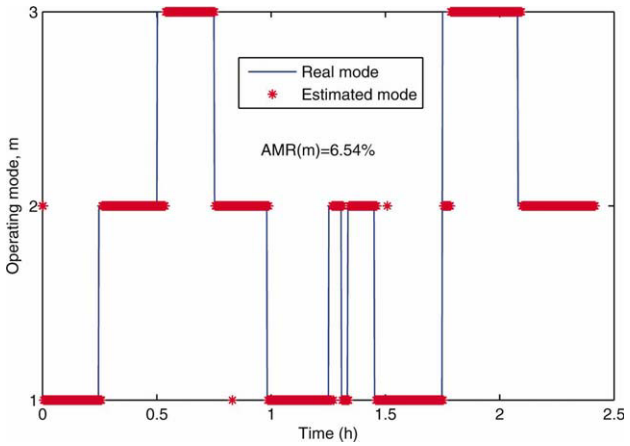

Figure 16. Noncontinuum state estimation: operating mode (m).

[Color figure can be viewed in the online issue, which is available at wileyonlinelibrary.com].

study, the nonlinear process model is detailed in the work of Olanrewaju et al.[11] However, the summarized hybrid process model is given as follows:

$$\frac{dx_{i,j}}{dt} = f_m(x_{i,j}, y_{i,j}, V_m, R_m, F_m, z_m; \theta),\ T_i = g_m(x_{i,j}, \beta),$$
$$m = \{1, 2, \ldots, l, \ldots, M\}, \quad i = \{1, \ldots, N_s\},$$
$$j = \{1, \ldots, Nc - 1\}, \qquad (38)$$

where $x_{i,j}$ and T_i are the liquid composition of MeOH (mole fraction) and temperature on the stage i respectively. V_m (kmol/h) is the vapor boil up; R_m (kmol/h) is the reflux flow rate; F_m (kmol/h) is the feed flow rate; z_m is the feed composition while T_i is the temperature on stage i. By selecting a suitable sampling time, the hybrid dynamic model of a distillation process can be discretized and expressed in the form of 1.

The state estimation problem in this experimental work is to infer the composition of the methanol (i.e., the continuum state) in the distillate product using the available stage temperature measurements. In this study, a change in the system operating mode is caused by a change in the vapor boil up (V, kmol/h) with an unknown switching transition function. However, this transition function follows a hidden Markov model during the experiment. Figures 8 and 9 compare the steady state conditions of the three different operating modes as obtained from the experiment to those predicted by the process model. The results show that the predicted steady state profiles are able to capture the change in the system operating modes with a change in the column vapor boil up. The operating condition parameters for these three different modes are given in Table 3, while the hidden Markov model parameters are provided in Appendix D.

To test the performances of the proposed HMHE, measurements of temperature from the thermocouples located on all of the column stages except the condenser are obtained at every 10 s and fed into the estimator online. Figures 10–13 show the performance of the HMHE in estimating the distillate product composition as well as the unknown switching

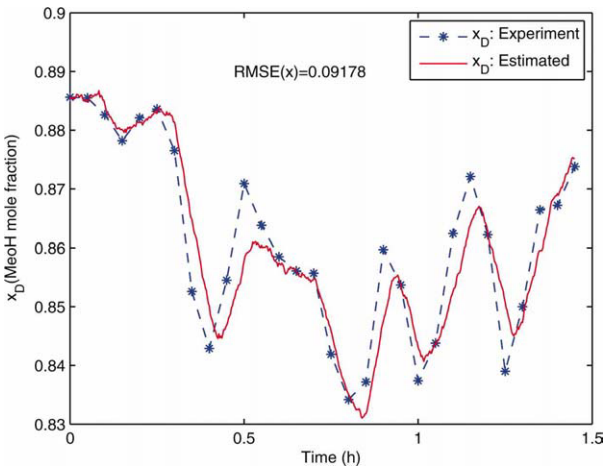

Figure 15. Continuum state estimation: Composition of MeOH in the distillate product.

[Color figure can be viewed in the online issue, which is available at wileyonlinelibrary.com].

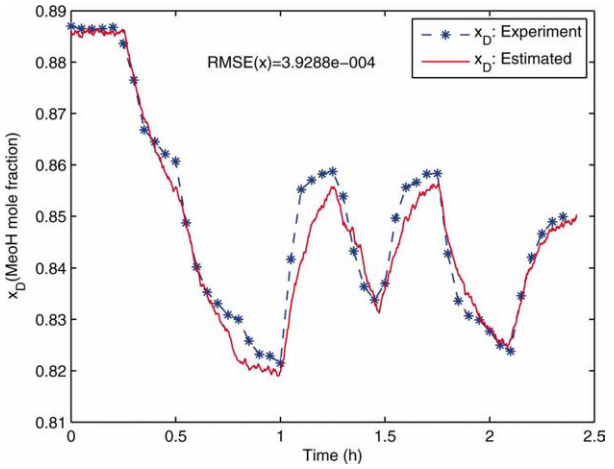

Figure 17. Continuum state estimation: Composition of MeOH in the distillate product.

[Color figure can be viewed in the online issue, which is available at wileyonlinelibrary.com].

Table 4. Effects of Constraints on the HMHE Performance

	AMR (%)	RMSE (x)	CPU Time (min)
Constraints	6.54	3.9281×10^{-4}	54
No constraints	7.25	3.9692×10^{-4}	81

operating modes. The continuum state dynamics shown in Figure 11 corresponds to the switch in operating modes shown in Figure 10, while the continuum state dynamics of Figure 13 follows a different switching modes shown in Figure 12. If we compare the two switching patterns, one can see that the HMHE performance is better (i.e., lower AMR(m)) in the results shown in Figures 10 and 11 than those shown in Figures 12 and 13. This is because the switching time is fairly constant and much longer in Figure 10 than that in Figure 12.

The HMHE performance is also tested using a different HMM parameters (see Appendix E), in which the switching pattern is much irregular with a faster switching time. The results are shown in Figures 14 and 15. Even though the HMHE is able to capture the general trend of MeOH composition dynamics as well as the switching operating mode, the MHE performance in this case is poorer than the previous results. The reason for this is because the rate of switching between one operating mode and another, in some instances, becomes faster than the natural system dynamics, i.e., switching occurs before the process settles to a steady state. Under this condition, the assumption of treating a change vapor boil up as a discrete-event state (i.e., sudden jump with no transition between operating modes) will no longer be valid. From practical point of view, HMHE will perform well as long as the rate of switching from one operating mode into another is slower than the system dynamics.

Effect of Incorporating Constraints. To assess the performance of the HMHE when using the available information about the controlled input variable (i.e., Reflux flow rate) and the process states (i.e., stage compositions) in constraining both the continuum state as well as the noncontinuum state space, the following constraints are considered in HMHE implementation:

(1) Continuum state constraint:

$$0 \leq x_{i,j} \leq 1, \tag{39}$$

(2) Noncontinuum state space constraint:

$$R_m(k) < \bar{R}_m, \quad m_k \in M_i : \quad M_i = 2, \tag{40}$$

$$R_m(k) \geq \bar{R}_m, \quad m_k \in M_i : \quad M_i = 3. \tag{41}$$

where $\overline{R}_m$ is the steady state reflux flow rate given in Table 3. Figures 16 and 17 show the performance of HMHE in estimating the operating mode (i.e., noncontinuum state) and the distillate composition (i.e., continuum state) when the constraints are included. The performances of HMHE when the constraints are incorporated are quantitatively compared with when there are no constraints, and the results are summarized in Table 4. The AMR, RMSE, as well as the computational time are much lower with better estimate of the states when the constraints are imposed.

In this work, major efforts are directed into the HMHE algorithm development, implementation and its potential engineering applications with the stability and convergence examined and conjectured only through simulation and experimental studies. The convergence of HMHE has not been theoretically proven and would be explored in our future studies.

Conclusion

A HMHE for simultaneous continuum and noncontinuum state estimation in a constrained switching dynamic system is developed. We have shown that a hybrid state estimation, which is based on a moving horizon optimization technique, is a powerful tool in which further information about the system can be incorporated in estimation through constraints on both the continuum and noncontinuum states. A generalized arrival cost, which accounts for the cost due to mode transition states as well as due to the continuum state dynamics is derived for HMHE. A series of experimental studies on a distillation column separating methanol-isopropanol mixture have shown that HMHE performs well in estimating both the continuum and noncontinuum states simultaneously.

Literature Cited

1. Boers Y, Driessen H. Hybrid state estimation: a target tracking application. *Automatica*. 2002;38:2153–2158.
2. Hu Y, El-Farra NH. Robust fault detection and monitoring of hybrid process systems with uncertain mode transitions. *AIChE J*. 2010.
3. Balluchi A, Benvenuti L, Benedetto MD, Sangiovanni-Vincentelli AL. Hybrid control of force transients for multi-point injection engines. *Int. J. Robust Nonlinear Control*. 2001;11:515–539.
4. Mhaskar P, El-Farra NH, Christofides PD. Predictive control of switched nonlinear systems with scheduled mode transitions. *IEEE Trans Automat Control*. 2005;50:1670–1680.
5. El-Farra NH, Mhaskar P, Christofides PD. Output feedback control of switched nonlinear systems using multiple Lyapunov functions. *Syst Control Lett*. 2005;54:1163–1182.
6. Bemporad A, Mignone D, Morari M. Moving horizon estimation for hybrid systems and fault detection. *Proceedings of American Control Conference*, San Diego, CA, 1999:2471–2475.
7. Alessandri A, Coletta P. Switching observers for continuous-time and discrete-time linear systems. *American Control Conference*, Arlington, VA, 2001:2516–2521.
8. Alessandri A, Coletta P. Design of observers for switched discrete-time linear systems. *American Control Conference*, Denver, CO, 2003:2785–2790.
9. Böker G, Lunze J. Stability and performance of switching Kalman filters. *Int J Control*. 2002;75:1269–1281.
10. Hofbaur MW, Williams BC. Hybrid estimation of complex Systems. *IEEE Trans System Man Cybernet Part-B Cybernet*. 2004;34:2178–2191.
11. Olanrewaju MJ, Huang B, Afacan A. Online composition estimation and experiment validation of distillation processes with switching dynamics. *Chem Eng Sci*. 2010;65:1597–1608.
12. Rao CV, Rawlings JB. Constrained process monitoring: moving horizon approach. *AIChE J*. 2002;48:97–109.
13. Ferrari-Trecate G, Mignone D, Morari M. Moving horizon estimation for hybrid systems. *Proceedings of American Control Conference*. Chicago, IL, 2000:1684–1688.
14. Ferrari-Trecate G, Mignone D, Morari M. Moving horizon estimation for hybrid systems. *IEEE Trans Automat Control*. 2002;47:1663–1676.
15. Pina L, Botto MA. Simultaneous state and input estimation of hybrid systems with unknown inputs. *Automatica*. 2006;42:755–762.
16. Rowe C, Maciejowski J. Min-max moving horizon estimation for a class of hybrid systems. *Proceedings of the 42nd IEEE Conference on Decision and Control*, Maui, Hawai, 2003:149–154.
17. Alessandri A, Baglietto M, Battistelli G. Minimum-distance receding-horizon state estimation for switching discrete-time linear system. In:

Findeisen R, et al., editor. *Assessment and Future Directions*, LNCIS 358. Heidelberg, Germany: Springer-Verlag, 2007:347–358.
18. Qu CC, Hahn J. Computation of arrival cost for moving horizon estimation via unscented Kalman filtering. *J Process Control*. 2009;19:358–363.
19. Ungarala S. Computing arrival cost parameters in moving horizon estimation using sampling based filters. *J Process Control*. 2009;19:1576–1588.
20. Jacobsen EJ, Skogestad S. Dynamics and control of unstable distillation columns. *Modeling Identification Control*. 1993;14:59–72.
21. Wang J. Complex dynamics in a nonlinear chemical system switching between two stable stationary states. *J Chem Phys*. 2003;11:3626–3630.
22. Rabiner LR. A tutorial on hidden Markov models and selected applications in speech recognition. *Proc IEEE*. 1989;77:257–286.
23. Floudas CA, Visweswaran V. A global optimization algorithm (GOP) for certain classes of nonconvex NLPs I. Theory. *Comput Chem Eng*. 1990;14:1397–1417.
24. Gendron B, Cranic, TG. Parallel branch-and-bound algorithms: survey and synthesis. *Oper Res*. 1994;42:1042–1066.
25. Bernhard H, Korte BH, Vygen J. *Combinatorial Optimization: Theory and Algorithms*, 4th ed. Heidelberg: Springer-Verlag, 2008.
26. Duran MA, Grossmann IE. An outer approximation algorithm for a class of mixedinteger nonlinear programs. *Math Programm*. 1986;36:307–339.
27. Viswanathan J, Grossamann IE. A combined penalty function and outer-approximation method for MINLP optimization. *Comput Chem Eng*. 1990;14:769–782.
28. Geoffrion AM. Generalized benders decomposition. *J Optim Theory Appl*. 1972;10:237–260.
29. Mejdell T, Skogestad S. Composition estimator in a pilot-plant distillation column using multiple temperatures. *Ind Eng Chem Res*. 1991;30:2555–2564.
30. Baratti R, Bertucco A, Alessandro D, Morbidelli M. Development of a composition estimator for binary distillation columns. Application to a pilot plant. *Chem Eng Sci*. 1995;50:541–1550.
31. Baratti R, Bertucco A, Alessandro D, Morbidelli M. A composition estimator for multicomponent distillation columns development and experimental test on ternary mixtures. *Chem Eng Sci*. 1998;53:3601–3612.
32. Kiva VN, Alukhanova BM. Multiple steady states of distillation and its realisation. *Comput Chem Eng*. 1997;21:S541–S546.
33. Rios-Bolivar A, Szigeti F. Binary distillation column control based on state and input observability. *Proc. of the 10th Mediterranean Conference on Control and Automation*, Lisbon, Portugal, 2002.

Appendix A

Given 9 as

$$\min_{\hat{m}_{T-N:T},\ \hat{x}_{T-N:T}} \{J_T\}: \quad J_T = \phi_{T-N} + J_{T-N+1:T}, \tag{A1}$$

where

$$J_{T-N+1:T} = -\ln\ P(x_{T-N+1:T}, m_{T-N+1:T}, y_{T-N+1:T}|x_{T-N}, m_{T-N}), \tag{A2}$$

the joint probability distribution of the noncontinuum state $m_{T-N+1:T}$ and the continuum state $x_{T-N+1:T}$ with the available measurement data $y_{T-N+1:T}$ can be expressed as

$$P(x_{T-N+1:T}, m_{T-N+1:T}, y_{T-N+1:T}|x_{T-N}, m_{T-N}) = \prod_{k=T-N+1}^{T} P(m_k|m_{k-1}) \prod_{k=T-N+1}^{T} P(x_k|x_{k-1}, m_k) \times \prod_{k=T-N+1}^{T} P(y_k|x_k, m_k). \tag{A3}$$

If we take the logarithm of 44 and make use of $J_{T-N+1:T}$ as defined in A2, then, A1 becomes

$$\min_{\hat{m}_{T-N:T},\ \hat{x}_{T-N:T}} \{J_T\}: \quad J_T = \phi_{T-N} - \sum_{k=T-N+1}^{T} \ln P(m_k|m_{k-1}) - \sum_{k=T-N+1}^{T} \ln P(x_k|x_{k-1}, m_k) - \sum_{k=T-N+1}^{T} \ln P(y_k|x_k, m_k). \tag{A4}$$

If we assume that the continuum state x_k and the observation state y_k follow a Gaussian distribution, A4 can further be subdivided and defined as follows:

• Given the mode m_k and the state x_{k-1}, the conditional probability distribution of the state x_k with mean of $f_{m_k}(x_{k-1}, u_{k-1}; \theta)$ and covariance matrix of Q_k is:

$$P(x_k|x_{k-1}, m_k) = (2\pi)^{-n/2} {Q_k}^{-1/2} \times \exp\left[-\frac{1}{2}\{x_k - f_{m_k}(x_{k-1}, u_{k-1}; \theta)\}^T \times {Q_k}^{-1}\{x_k - f_{m_k}(x_{k-1}, u_{k-1}; \theta)\}\right], \tag{A5}$$

• Conditioned on the mode m_k and x_k, the probability distribution of the observation y_k with the mean of $g_{m_k}(x_k; \beta)$ and covariance matrix of R_k is:

$$P(y_k|x_k, m_k) = (2\pi)^{-q/2} {R_k}^{-1/2} \times \exp\left[-\frac{1}{2}\{y_k - g_{m_k}(x_k; \beta)\}^T {R_k}^{-1}\{y_k - g_{m_k}(x_k; \beta)\}\right]. \tag{A6}$$

If we define the following terms:

$$\hat{w}_{k-1} = \hat{x}_k - f_{\hat{m}_k}(\hat{x}_{k-1}, u_{k-1}; \theta), \quad \hat{v}_k = y_k - g_{\hat{m}_k}(\hat{x}_k; \beta), \tag{A7}$$

and by taking the negative logarithm of A5 and A6, we have

$$-\ln P(x_k|m_k) = \mathbf{B}_k + \frac{1}{2}\hat{w}_{k-1}^T {Q_k}^{-1}\hat{w}_{k-1}, \tag{A8}$$

$$-\ln P(y_k|x_k, m_k) = \mathbf{C}_k + \frac{1}{2} v_k^T {R_k}^{-1} v_k, \tag{A9}$$

where $\mathbf{B}_k = -\ln(2\pi)^{-n/2} {Q_k}^{-1/2}$ and $\mathbf{C}_k = -\ln(2\pi)^{-\frac{q}{2}}\ {R_k}^{-1/2}$. If we define $\gamma_{k-1}^{(i)}$, $\alpha_k^{(j)}$ and $\mathbb{P}_{k-1,k}^{(i,j)}$ as

$$\gamma_{k-1}^{(i)} = \begin{cases} 1 & \text{if } i = \hat{m}_{k-1} \\ 0 & \text{if } i \neq \hat{m}_{k-1}, \end{cases} \tag{A10}$$

$$\alpha_k^{(j)} = \begin{cases} 1 & \text{if } j = \hat{m}_k \\ 0 & \text{if } j \neq \hat{m}_k, \end{cases} \tag{A11}$$

and

$$\mathbb{P}_{k-1,k}^{(i,j)} := P(m_k = j|m_{k-1} = i), \text{ for } i, j \in \mathbb{M}, \tag{A12}$$

respectively, we can obtain 10 by substituting A8 to A12 in A4 as

$$\min_{\{\hat{m}_{T-N:T},\ \hat{w}_{T-N:T}\}} J_T: \quad J_T = \phi_{T-N} - \sum_{k=T-N+1}^{T}\sum_{i=1}^{M}\sum_{j=1}^{M}\gamma_{k-1}^{(i)}\alpha_k^{(j)} \ln \mathbb{P}_{k-1,k}^{(i,j)} + \sum_{k=T-N}^{T-1}\sum_{j=1}^{M}\alpha_k^{(j)}\hat{w}_k^T Q_k{}^{-1}\hat{w}_k + \sum_{k=T-N+1}^{T}\sum_{j=1}^{M}\alpha^{(j)}\hat{v}_k^T R_k{}^{-1}\hat{v}_k + \mathbf{A}_k, \quad \text{(A13)}$$

where $\mathbf{A}_k = \mathbf{B}_k + \mathbf{C}_k$. Note that $\mathbf{A}_k$ is independent of the decision variables $\hat{m}_{T-N:T}$ and $\hat{w}_{T-N:T}$ and can be neglected in A13.

Appendix B

Given the following:

$$\phi_k^x = -\ln P(x_k|m_k, y_{0:k}). \quad \text{(B1)}$$

Proof. Using Bayesian rule, $P(x_k|m_k,y_{0:k})$ can be written as

$$P(x_k|y_{0:k}, m_k) = \frac{P(x_k|m_k)P(y_{0:k}|x_k, m_k)}{P(y_{0:k}|m_k)}, \quad \text{(B2)}$$

which can also be written as

$$P(x_k|y_{0:k}, m_k) = \mathbf{D}_k P(x_k|m_k)P(y_{0:k}|x_k, m_k), \quad \text{(B3)}$$

where $\mathbf{D}_k = P(y_{0:k}|m_k)^{-1}$. Using the conditional independency properties (see Figure 1):

$$P(x_k|y_{0:k}, m_k) = \mathbf{D}_k P(x_k|m_k)P(y_k|x_k, m_k). \quad \text{(B4)}$$

Then, B1 becomes

$$\phi_k^x = -\ln \mathbf{D}_k - \ln P(x_k|m_k) - \ln P(y_k|x_k, m_k). \quad \text{(B5)}$$

Following the same derivations and analysis in Appendix A, it is straightforward to see that both the second and the third term of B5 will become

$$-\ln P(x_k|m_k) = \mathbf{B}_k + \frac{1}{2}\hat{w}_{k-1}^T P_k{}^{-1}\hat{w}_{k-1}, \quad \text{(B6)}$$

and

$$-\ln P(y_k|x_k, m_k) = \mathbf{C}_k + \frac{1}{2}v_k^T R_k{}^{-1}v_k, \quad \text{(B7)}$$

Hence,

$$\phi_k^x = \frac{1}{2}w_{k-1}^T P_k{}^{-1}w_{k-1} + \frac{1}{2}v_k^T R_k{}^{-1}v_k + \mathbf{E}_k, \quad \text{(B8)}$$

where $\mathbf{E}_k = \mathbf{B}_k + \mathbf{C}_k - \ln\mathbf{D}_k$.

Appendix C

The parameters of the switching linear system of A4 are given as follows:

$$F^{(1)} = \begin{pmatrix} -0.211 & 0 \\ 0 & 0.521 \end{pmatrix}, F^{(2)} = \begin{pmatrix} 0.691 & 0 \\ 0 & -0.310 \end{pmatrix}, F^{(3)} = \begin{pmatrix} 0.153 & 0 \\ 0 & 0.410 \end{pmatrix}, \quad \text{(C1)}$$

$$B^{(1)} = B^{(2)} = B^{(3)} = \begin{pmatrix} -2 \\ 1 \end{pmatrix}, \quad \text{(C2)}$$

$$H^{(1)} = H^{(2)} = H^{(3)} = \begin{pmatrix} 1 & 0 \\ 0 & 1 \end{pmatrix}. \quad \text{(C3)}$$

The transition probability matrix $\mathbb{P}$ is given as,

$$\mathbb{P} = \begin{pmatrix} 0.90 & 0.05 & 0.05 \\ 0.05 & 0.90 & 0.05 \\ 0.05 & 0.05 & 0.90 \end{pmatrix}. \quad \text{(C4)}$$

when the constraint on the space span M_i as given in 36 is not active and

$$\mathbb{P} = \begin{pmatrix} 0.95 & 0.05 \\ 0.05 & 0.95 \end{pmatrix}. \quad \text{(C5)}$$

when the constraint on the space span M_i as given in 36 is active.

Appendix D

$$\mathbb{P} = \begin{pmatrix} 0.9914 & 0.0058 & 0.0029 \\ 0.0083 & 0.9875 & 0.0042 \\ 0.0048 & 0.0048 & 0.9905 \end{pmatrix}. \quad \text{(D1)}$$

Appendix E

$$\mathbb{P} = \begin{pmatrix} 0.9805 & 0.0078 & 0.0117 \\ 0.0196 & 0.9706 & 0.0098 \\ 0.0184 & 0.0061 & 0.9755 \end{pmatrix}. \quad \text{(E1)}$$

Manuscript received Nov. 12, 2010, and revision received Feb. 1, 2011.